Perovskite Solar Cells Prepared by a New 3-step Method Including a PbI_2 Scavenging Step

Yuji Okamoto[†] and Yoshikazu Suzuki[*1‡]

[†]Graduate School of Pure and Applied Sciences, University of Tsukuba, Ibaraki 305-8573, Japan

[‡]Faculty of Pure and Applied Sciences, University of Tsukuba, Ibaraki 305-8573, Japan

Abstract: $CH_3NH_3PbI_3$ films prepared by the 2-step method for perovskite solar cells generally have problems of residual unreacted PbI_2 and rough surface structure. Here, we report a new 3-step method, based on the 2-step method with an additional spin-coating of CH_3NH_3(I,Br) solution on the $CH_3NH_3PbI_3$ film to scavenge remnant PbI_2. The 3-step method improved light absorption of the film by converting the residual PbI_2 into $CH_3NH_3PbI_{3-x}Br_x$. Morphological improvements such as a network formation among perovskite grains and a decrease of intergranular voids were also observed. The additional CH_3NH_3I spin-coating resulted in the increases of both J_{SC} and V_{OC}, while that of CH_3NH_3Br solution showed a slight decrease of J_{SC} and large increase of V_{OC} due to the enlarged bandgaps. The maximum power conversion efficiency was improved from 12.9 % (2-step) to 14.4 % (3-step). Furthermore, the 3-step cells retained ~85 % of the original PCE values after storing in air for 700 h, which indicates an improved stability.

[1] Corresponding author: Faculty of Pure and Applied Sciences, University of Tsukuba, Ibaraki 305-8573, Japan.

E-mail address: suzuki@ims.tsukuba.ac.jp (Y. Suzuki).

1. Introduction

After the first report about the perovskite solar cells in 2009 [1], various preparation processes for perovskite-type $CH_3NH_3PbX_3$ active layers (X: I, Br or Cl) were reported [2-9]. Spin-coating process for the perovskite layer is an easy wet-chemical process, and it is more popular than dry processes such as chemical vapor deposition (CVD) [10,11] and pulse laser deposition (PLD) [12]. The spin-coating process for the perovskite solar cells is usually categorized into 1-step and 2-step methods [13]. The 1-step method, i.e. one time spin-coating of a precursor solution composed of PbI_2, CH_3NH_3I and organic solvent, initially had a problem of a poor coverage of the perovskite film [14,15]. To solve this problem, some improved 1-step processes have been proposed such as solvent vapor assisting method [2,16] and anti-solvent dripping method [3,4].

Meanwhile, the 2-step method, i.e. pre-coating of PbI_2 film and post-conversion to $CH_3NH_3PbI_3$ by reacting with a CH_3NH_3I solution, is suitable to prepare the well-covered perovskite film. However, the 2-step method also has some problems of (1) residual unreacted PbI_2 [17-19] and (2) rough surface structure of the perovskite film [20]. To improve the 2-step method, some research groups have tried to develop modified 2-step methods, e.g., the in situ method by Xiao et al., resulting in a high power conversion efficiency (PCE) of 12.22 % even without a hole transport material [7-9].

The effect of residual unreacted PbI_2 on the performance of perovskite solar cells is still unclear. As a positive effect of residual PbI_2, Cao et al. [17] reported that the residual PbI_2 decreased a carrier back transfer due to the band position of PbI_2. Meanwhile, as a negative effect, Jacobsson et al. [18] and Kwon et al. [19] reported that the residual PbI_2 reduced the open circuit voltage (V_{OC}) and short circuit current density (J_{SC}), respectively. Considering these

results, a large amount of residual PbI_2 should be avoided. The residual PbI_2 can be decreased by (i) prolonging the dipping time in the CH_3NH_3I solution and (ii) increasing the concentration of the CH_3NH_3X solution. However, the performance of perovskite solar cells often decreased with those methods due to (i) the damage to the $CH_3NH_3PbI_3$ particles by the solvent and (ii) the decrease of $CH_3NH_3PbI_3$ particle size, respectively [17,21,22].

A post-treatment of CH_3NH_3X solution (X: I or Br) is a potential method to decrease the residual PbI_2 and to improve the perovskite film morphology. Zhu et al. [23] reported the decrease of residual PbI_2 by loading CH_3NH_3Br (MABr) solution on the 2-step $CH_3NH_3PbI_3$ film and the enhancement of PCE. However, longer liquid-loading time possibly damages $CH_3NH_3PbI_3$ film due to the dissolution in the CH_3NH_3X solution [24]. The liquid-loading time would be better to be minimized. Meanwhile, Yang et al. [25] have recently reported the conversion of a low quality 1-step $CH_3NH_3PbI_3$ film into a high quality pinhole-less $CH_3NH_3PbI_{3-x}Br_x$ film with large grain size by the additional spin-coating of MABr solution (via the Ostwald ripening process).

Here, we report a new 3-step method, based on the 2-step method with an additional spin-coating of $CH_3NH_3(I,Br)$ solution on the $CH_3NH_3PbI_3$ film to scavenge remnant PbI_2. The additional spin-coating of a CH_3NH_3X solution on the 2-step $CH_3NH_3PbI_3$ film is expected to improve the cell performance by decreasing the residual PbI_2 (similarly to Ref. 23) and to improve the film morphology (as of Ref. 25), with the minimum damage on the perovskite film via the shorter liquid-loading time. Via the 3-step method, i.e. with the additional spin-coating treatment, the residual PbI_2 was successfully reduced and the smoother perovskite films with fewer intergranular voids were achieved, which resulted in the enhanced photovoltaic performance and improved stability in air.

2. Experimental section

2.1. Preparation of TiO_2 compact and mesoporous layer

Transparent conductive oxide (TCO, Type-0052, 10 Ω/sq., Geomatec) substrates were patterned by etching with Zn powder (>96.0 %, Tokyo Chemical Industry) and 1 M HCl (Wako Pure Chemical Industry). The substrates were cleaned by ultrasonication in ethanol for 5 min and dried. The TiO_2 compact layers were prepared by spray-pyrolysis method; a 0.15 M titanium diisopropoxide bis (acetylacetonate) (75 % in isopropanol, Sigma-Aldrich) solution in ethanol was sprayed on the patterned substrates with heating at 500°C. TiO_2 mesoporous layers were then prepared by spin-coating a TiO_2 paste (18NR-T, Dyesol), which was diluted in ethanol at the weight ratio of 1:5, on the substrates at 4000 rpm for 25 s and annealed at 500°C for 30 min. The coated substrates were immerged in a 40 mM $TiCl_4$ (99.0 %, Wako Pure Chemical Industry) solution in distilled water at 70°C for 30 min, followed by rinsing with ethanol and annealing at 500°C for 30 min.

2.2. Preparation of perovskite active layer, hole transport layer and metal electrode

The perovskite active layer and hole transport layer (HTL) were prepared in air with humidity of ~30 %. The preparation process of perovskite active layer is depicted in **Figure 1**. The TiO_2 coated substrates were pre-heated at 60°C, and 1 M PbI_2 (>98.0 %, Tokyo Chemical Industry) solution in N,Ndimethylformamide (DMF, 99.5 %, Nacalai tesque), which was pre-heated at 60°C, was spin-coated on the substrates at 3000 rpm for 20 s (i.e. the 1st step). After annealing at 60°C for 10 min, the substrates were dipped in a 10 mg mL^{-1} CH_3NH_3I (MAI, 98 %, Wako Pure Chemical Industry) solution dissolved in 2-propanol for 20 s, followed by rinsing

with 2-propanol and annealing at 60°C for 10 min (i.e. the 2nd step). Then, 20 μL of MAI solution (20 mg mL^{-1}), CH_3NH_3Br (MABr, 98 %, Wako Pure Chemical Industry) solution (14 mg mL^{-1}) or mixed solution of MAI (10 mg mL^{-1}) and MABr (7 mg mL^{-1}) were dispersed on the prepared $CH_3NH_3PbI_3$ films during the spinning at 4000 rpm for 35 s (i.e. the 3rd step). The treated substrates were annealed at 60°C for 10 min, and then, the HTLs with the thickness of ~100 nm were prepared by spin-coating a spiro-MeOTAD solution at 4000 rpm for 35 s. The spiro-MeOTAD solution was composed of 73 mg spiro-MeOTAD (99%, Sigma-Aldrich), 28.8 μL 4-*tert*-butylpyridine (TBP, 96.0 %, Sigma-Aldrich) and 17 μL a solution of 520 mg mL^{-1} lithium bis(trifluoromethylsulphonyl)imide salt (98.0%, Tokyo Chemical Industry) in acetonitrile (99.5 %, Wako Pure Chemical Industry) in 1 mL chlorobenzene (99 %, Nacalai tesque) . Finally, Ag electrodes with the thickness of ~50 nm were deposited on the HTLs with a thermal evaporator under 3×10^{-5} Torr.

2.3. Characterizations

Constituent phases of the prepared perovskite films were characterized by X-ray diffraction (XRD, Multiflex, Cu-K_α, 40 kV and 40 mA, Rigaku). Optical absorbance and transmittance of the prepared cells were measured by ultraviolet-visible absorption spectroscopy (UV-Vis, UV-1280, Shimadzu). The surface morphology and cross section of the ETLs and perovskite active layers were observed using scanning electron microscopy (SEM, JSM-5600LV and SU-8020, JEOL and Hitach High-technologies). Current density-voltage (*J-V*) characteristics were measured by using a solar simulator (XES-40S1, SAN-EI Electric), which was calibrated to AM 1.5, 100 mW/cm^2 with a standard silicon photodiode (BS-520BK, Bunkokeiki). The voltage

step and delay time were 20 mV and 50 ms, respectively. The active area was limited to 0.087 cm^2 by using black mask.

3. Results

3.1. Phase analysis

Figure 2 shows XRD patterns of the prepared solar cells at 2θ=10-70° and enlarged ones at 2θ=27.5-29.0°. Although the residual PbI_2 peaks at ~12.5° and ~38° were observed in all the cells, the intensity of PbI_2 peaks decreased and those for perovskite increased by the additional spin-coating (3rd step), which indicates the conversion of residual PbI_2 into perovskite phase. The amount of residual PbI_2 can be controlled by changing the concentration of additional spin-coating CH_3NH_3X solutions. The peaks at ~28.0° and ~28.3° in the additionally MAI spin-coated cell correspond to the (004) and (220) planes of tetragonal $CH_3NH_3PbI_3$ [26]. The peak of (004) plane is not obvious in the cell without additional spin-coating (2-step only cell), which is attributable to the smaller intensity for peaks of the $CH_3NH_3PbI_3$ and larger background than that for additionally MAI spin-coated cell. With the additional spin-coating of MA(I,Br) and MABr solution, the 220 peaks were shifted to larger angle and 004 peak intensities became smaller. This indicates the formation of $CH_3NH_3PbI_{3-x}Br_x$ [26-29].

3.2. Optical properties

Figure 3a shows absorbance spectra of the perovskite active layers in the range of 600-800 nm. The bandgaps were estimated from the absorption onset by using the Tauc plot. The absorbance showed rapid increase around wavelength of ~780 nm for the 2-step only cell, and the bandgap was estimated to be 1.60 eV. This is comparable value with some reported bandgaps

of $CH_3NH_3PbI_3$ [28,30]. The onset of absorbance for the additionally MAI spin-coated cell with the bandgap of 1.61 eV was comparable to that for 2-step only cell. On the other hand, the bandgap blue-shifted to 1.64 eV for the additionally MA(I,Br) spin-coated cell and 1.68 eV for the additionally MABr spin-coated cell due to the synthesis of $CH_3NH_3PbI_{3-x}Br_x$. Furthermore, we estimated the value of x (viz. concentration of Br) in $CH_3NH_3PbI_{3-x}Br_x$ for additionally MA(I,Br) and MABr spin-coated cells by using the following equation.

$$E_g(x) = E_g(CH_3NH_3PbBr_3)\frac{x}{3} + E_g(CH_3NH_3PbI_3)\left(1 - \frac{x}{3}\right) - \frac{x}{3}\left(1 - \frac{x}{3}\right)b \quad (1)$$

The b is a bowing constant. The equation can be rearranged as reported in the previous study [28].

$$E_g(x) = 1.598 + 0.36\left(\frac{x}{3}\right) + 0.34\left(\frac{x}{3}\right)^2 \quad (2)$$

The x of additionally MA(I,Br) spin-coated cell was estimated to be 0.32 (i.e. $CH_3NH_3PbI_{2.68}Br_{0.32}$) and that for additionally MABr spin-coated cell was estimated to be 0.56 (i.e. $CH_3NH_3PbI_{2.44}Br_{0.56}$), respectively.

Figure 3b shows the transmittance of the prepared perovskite active layers. The additionally spin-coated cells showed smaller transmittance than that for the 2-step only cell, which indicates a better light absorption, at the shorter wavelength range than that corresponding to the bandgaps. This is ascribed to the additionally synthesized $CH_3NH_3PbI_{3-x}Br_x$ from the residual PbI_2. On the other hand, the transmittance of the additionally MA(I,Br) spin-coated cell at ~740-800 nm and additionally MABr spin-coated cell at ~720-800 nm were larger than that for the 2-step only cell due to the larger bandgaps.

3.3. Morphology of perovskite active layer

Figures 4a-c show top view SEM images of the perovskite active layers: (a) 2-step only, (b) additionally MAI spin-coated and (c) additionally MABr spin-coated cells. The diameter of the perovskite particles were ~500 nm-1 μm in all the cells. After the additional spin-coating, the edge of $CH_3NH_3PbI_3$ particles became somewhat roundish. Furthermore, the particles partially connected to each other, and a network among the perovskite particles was also observed (see red arrows). **Figures 4d-f** show cross-sectional SEM images of the perovskite active layers: (d) 2-step only, (e) additionally MAI spin-coated and (f) MABr spin-coated cells. The mp-TiO_2/$CH_3NH_3PbI_{3-x}Br_x$ and $CH_3NH_3PbI_{3-x}Br_x$ capping layers were observed in all the cells, which have the comparable thickness. The surface of capping layer for 2-step only cell was relatively rough due to the $CH_3NH_3PbI_3$ particles with the sharp edge. After the additional spin-coating of MAI and MABr solution, the surface of capping layer became smoother and the intergranular voids became filled, which is ascribed to the dissolution of $CH_3NH_3PbI_3$ particles at the surface.

3.4. Photovoltaic performance and *J-V* hysteresis

Figure 5a shows typical *J-V* curves (back scan) of the prepared solar cells measured on just after the preparation. The detail values (average of 8 cells) are listed in **Table 1**. The 2-step only cell displayed the J_{SC} of 21.2 mA/cm^2, V_{OC} of 0.91 V, *FF* of 0.66 and power conversion efficiency (PCE) of 12.9 %. With the additional MAI spin-coating, J_{SC} and V_{OC} increased to 22.1 mA/cm^2 and 0.94 V, respectively, and the larger PCE of 14.4 % was achieved. J_{SC} decreased and V_{OC} increased with increasing the Br ratio of additional spin-coating solution compared with the additionally MAI spin-coated cell. J_{SC} of 20.8 mA/cm^2, V_{OC} of 0.95 V, *FF* of 0.71 and PCE of 14.2 % for the additionally MA(I,Br) spin-coated cell and J_{SC} of 19.5 mA/cm^2, V_{OC} of 0.99 V,

FF of 0.70 and PCE of 13.5 % for the additionally MABr spin-coated cell were achieved. As a result, all the 3-step cells showed the enhanced PCE compared with the 2-step only cell. Therefore, the 3-step method in this study is effective to improve the photovoltaic performance of the perovskite solar cells. Although slight drops of current at around 0 V were observed for the 3-step cells (**Figure 5a)**, they almost disappeared after the storing 3 days in air with the humidity of ~30% (**Figure 5b**).

The typical *J-V* curves in forward scan measured on 3 days after the preparation are shown in **Figure 6**, and the detail values (average of 8 cells) are listed in **Table 2**. A relatively large hysteresis was confirmed in all the cells. As for the meso-super structure perovskite solar cells, some researchers pointed out that the hysteresis becomes larger by decreasing the thickness of mesoporous layer, and relatively large hysteresis was observed for less than ~200 nm [31,32]. Our solar cells have the TiO_2 mesoporous layers with the thickness of ~150 nm as shown in **Figures 4d-f.** The observed hysteresis can be suppressed by increasing the thickness of mesoporous layer.

3.5. Stability in air

We also investigated the stability of the 2-step only, additionally MAI spin-coated and MABr spin-coated cells by storing the cells in air with the humidity of ~30% as shown in **Figure 7**. The PCE of the 2-step only cell kept decreasing after the preparation, and the PCE became less than 60 % of the original value at 700 h. On the other hand, the additionally spin-coated cells retained the original PCE values up to ~150 h, and they still showed more than 80 % even after 700 h. These results demonstrate that the 3-step method is effective to improve the stability of

perovskite active layer in air. The improved stability is attributable to the suppression of contact between moisture (in air) and the perovskite film due to the decrease of intergranular voids in the perovskite films via the additional spin-coating. Moreover, the excess CH_3NH_3X at the surface of the perovskite film may also contribute to suppress the contact of the moisture and the perovskite films.

4. Discussion

4.1. Microstructure development

The network formation of perovskite particles and the decrease of intergranular voids in the film were observed after the additional spin-coating. The microstructure development is attributable to the dissolution of perovskite particles at the surface into the additionally spin-coated CH_3NH_3X solution. It is reported that the $CH_3NH_3PbI_3$ particle growth in the 2-step method is due to the dissolution of the small particles in CH_3NH_3X solution and redeposition on the larger particles (Ostwald ripening growth) as a following reaction [21,24]:

$$CH_3NH_3PbI_3 + I^- \rightleftarrows CH_3NH_3^+ + PbI_4^{2-} \quad (3)$$

This scheme suggests that the surface of $CH_3NH_3PbI_3$ particles dissolve into the additionally spin-coated CH_3NH_3X solution. Then, the solution containing the dissolved $CH_3NH_3PbI_3$ will be dispersed during the spin-coating and partially bridge the particles, which results in the perovskite network and the decrease of intergranular voids. We also observed the surface of $CH_3NH_3PbI_3$ with the additional spin-coating of only 2-propanol as shown in **Figure S1**, and almost no morphological change was observed. This indicates that the morphological change takes place only with additional CH_3NH_3X spin-coating, which supports our results.

Some researchers observed the crystal growth of $CH_3NH_3PbI_3$ with the post-treatment of MABr solution due to the Ostwald ripening growth [23,25]. However, the crystal growth was not observed in our samples. Yang et al. [25] described that the penetration of MABr and the I/Br exchange reaction are dominant instead of the Ostwald ripening growth with the high concentrated MABr solution (> ~8 mg mL^{-1}). We used the relatively high concentrated MABr solution (14 mg mL^{-1}) to convert the residual PbI_2. Therefore, the additionally spin-coated CH_3NH_3X solution dissolved only the surface of $CH_3NH_3PbI_3$ particles without the crystal growth.

4.2. Additional coating effects on photovoltaic properties

For additionally MAI spin-coated cell, as shown in **Table 1**, J_{SC} was improved from 21.2 to 22.1 mA/cm^2 due to the enhanced light absorption by the additionally synthesized $CH_3NH_3PbI_3$. V_{OC} was also improved from 0.91 to 0.94 V possibly due to (1) the decrease of residual PbI_2, as is reported by Jacobsson et al., [18] and to (2) the suppression of carrier recombination in the smoother $CH_3NH_3PbI_3$ film with fewer intergranular voids, as shown in **Figures 4d-f** [33]. Next, for additionally MA(I,Br) spin-coated cell, J_{SC} (20.8 mA/cm^2) was comparable of the 2-step only cell (21.2 mA/cm^2) probably due to the balance of the positive effect of enhanced light absorption and the negative effect of enlarged band gap. V_{OC} was improved from 0.91 to 0.95 V due to (1) the decrease of residual PbI_2, (2) the suppression of carrier recombination, and also (3) larger band gap by Br substitution [23,26]. Finally, additionally MABr spin-coated cell, J_{SC} (19.5 mA/cm^2) was decreased from the 2-step only cell (21.2 mA/cm^2) due to the stronger negative effect of enlarged band gap. V_{OC} was much improved

from 0.91 to 0.99 V due to (1) the decrease of residual PbI_2, (2) the suppression of carrier recombination, and (3) stronger band gap effect.

4.3. Abnormal current drop around 0 V and curing 3 days later

In **Figure 5a**, the current drops around 0 V were observed for the additionally spin-coated cells, and the current drops disappeared on 3 days after the preparation. Since the current drop was not observed in the 2-step only cell, those for others can be caused by the morphological change of $CH_3NH_3PbI_{3-x}Br_x$ particles by the additional spin-coating (**Figures 4a-c**). To investigate the reason of the current-drop curing, we further conducted SEM observation on the perovskite active layers of 3 days after the preparation. **Figures S2** shows the top view SEM images of perovskite active layers: (a)-(c) just after the preparation (same as in **Figures 4a-c**) and (d)-(f) 3 days after the preparation. The morphology of the $CH_3NH_3PbI_3$ layer in the 2-step only cell was almost same between just and 3 days after the preparation (**Figure S2a and d**). On the other hand, as for the additionally MAI or MABr spin-coated cells, the necking points became somewhat thicker and the edges of $CH_3NH_3PbI_{3-x}Br_x$ particles became sharper for 3 days after the preparation (**Figures S2e-f**), which probably resulted in the current-drop curing.

5. Conclusions

Here, we have reported a new 3-step method, based on the 2-step method with an additional spin-coating of $CH_3NH_3(I,Br)$ solution on the $CH_3NH_3PbI_3$ film to scavenge remnant PbI_2. The additional spin-coating enhanced the light absorption of perovskite films by converting the residual PbI_2 into $CH_3NH_3PbI_{3-x}Br_x$, while shrinkage of absorbed light wavelength was also confirmed due to the enlarged bandgap. The formation of networks and decrease of intergranular

voids in the films were also observed by dissolving the surface of $CH_3NH_3PbI_3$ particles in the additionally spin-coated solutions. The additional MAI spin-coating increased both J_{SC} and V_{OC}, and the PCE was highly improved from 12.9 to 14.4 %. Although the additional MA(I,Br) and MABr spin-coating slightly decreased the J_{SC}, the enhancements of V_{OC} values were larger than that for the additionally MAI spin-coated cell, and improved PCEs of 14.2 % for the additionally MA(I,Br) spin-coated cell and 13.5 % for the additionally MABr spin-coated cell were achieved. Furthermore, the PCE degradations of the 3-step cells were less than half of that of the 2-step only cell, suggesting improved stability in air.

Author Contributions

The manuscript was written through contributions of all authors.

Notes

The authors declare no competing financial interest.

Acknowledgment

We thank the Kato Foundation for Promotion of Science for financial support.

References

[1] A. Kojima, K. Teshima, Y. Shirai, T. Miyasaka, Organometal Halide Perovskites as Visible-Light Sensitizers for Photovoltaic Cells. J. Am. Chem. Soc. 131 (2009) 6050–6051.

[2] Z. Xiao, Q. Dong, C. Bi, Y. Shao, Y. Yuan, J. Huang, Solvent Annealing of Perovskite-Induced Crystal Growth for Photovoltaic-Device Efficiency Enhancement. Adv. Mater. 26 (2014) 6503–6509.

[3] N. J. Jeon, J. H. Noh, Y. C. Kim, W. S. Yang, S. Ryu, S. I. Seok, Solvent Engineering for High-Performance Inorganic–Organic Hybrid Perovskite Solar Cells. Nat. Mater. 13 (2014) 897–903.

[4] M. Xiao, F. Huang, W. Huang, Y. Dkhissi, Y. Zhu, J. Etheridge, A. Gray-Weale, U. Bach, Y.-B. Cheng, L. A Spiccia, Fast Deposition-Crystallization Procedure for Highly Efficient Lead Iodide Perovskite Thin-Film Solar Cells. Angew. Chem. 126 (2014) 10056–10061.

[5] W. Nie, H. Tsai, R. Asadpour, J.-C. Blancon, A. J. Neukirch, G. Gupta, J. J. Crochet, M. Chhowalla, S. Tretiak, M. A. Alam, H.-L. Wang, A. D. Mohite, High-Efficiency Solution-Processed Perovskite Solar Cells with Millimeter-Scale Grains. Science 347 (2015) 522–525.

[6] J. Burschka, N. Pellet, S.-J. Moon, R. Humphry-Baker, P. Gao, M. K. Nazeeruddin, M. Grätzel, Sequential Deposition as a Route to High-Performance Perovskite-Sensitized Solar Cells. Nature 499 (2013) 316–319.

[7] Y. Xiao, G. Han, Y. Li, M. Li, Y. Changa, J. Wub, Preparation of High Performance Perovskite-sensitized Nanoporous Titanium Dioxide Photoanodes by in situ Method for Use in Perovskite Solar Cells. J. Mater. Chem. A 2 (2014) 16531.

[8] Y. Xiao, G. Han, Y. Li, M. Lia, J. Wu, Electrospun Lead-Doped Titanium Dioxide Nanofibers and the in situ Preparation of Perovskite-Sensitized Photoanodes for Use in High Performance Perovskite Solar Cells. J. Mater. Chem. A 2 (2014) 16856.

[9] Y. Xiao, G. Han, Y. Chang, Y. Zhang, Y. Li, M. Li, Investigation of Perovskite-Sensitized Nanoporous Titanium Dioxide Photoanodes with Different Thicknesses in Perovskite Solar Cells. J. Power Sources 286 (2015) 118.

[10] M. M. Tavakoli, L. Gu, Y. Gao, C. Reckmeier, J. He, A. L. Rogach, Y. Yao, Z. Fan, Fabrication of Efficient Planar Perovskite Solar Cells Using a One-Step Chemical Vapor Deposition Method. Sci. Rep. 5 (2015) 14083.

[11] M. Liu, M. B. Johnston, H. J. Snaith, Efficient Planar Heterojunction Perovskite Solar Cells by Vapour Deposition. Nature 501 (2013) 395−398.

[12] U. Bansode, R. Naphade, O. Game, S. Agarkar, S. Ogale, Hybrid Perovskite Films by a New Variant of Pulsed Excimer Laser Deposition: A Room-Temperature Dry Process. J. Phys. Chem. C. 119 (2015) 9177−9185.

[13] J. Cui, H. Yuan, J. Li, X. Xu, Y. Shen, H. Lin, M. Wang, Recent Progress in Efficient Hybrid Lead Halide Perovskite Solar Cells. Sci. Technol. Adv. Mater. 16 (2015) 036004.

[14] T. Salim, S. Sun, Y. Abe, A. Krishna, A. C. Grimsdalea, Y. M. Lam, Perovskite-Based Solar Cells: Impact of Morphology and Device Architecture on Device Performance. J. Mater. Chem. A 3 (2015) 8943–8969.

[15] G. E. Eperon, V. M. Burlakov, P. Docampo, A. Goriely, H. J. Snaith, Morphological Control for High Performance, Solution-Processed Planar Heterojunction Perovskite Solar Cells. Adv. Funct. Mater. 24 (2014) 151–157.

[16] Q. Chen, H. Zhou, Z. Hong, S. Luo, H.-S. Duan, H.-H. Wang, Y. Liu, G. Li, Y. Yang, Planar Heterojunction Perovskite Solar Cells via Vapor-Assisted Solution Process. J. Am. Chem. Soc. 136 (2014) 622−625.

[17] D. H. Cao, C. C. Stoumpos, C. D. Malliakas, M. J. Katz, O. K. Farha, J. T. Hupp, M. G. Kanatzidis, Remnant PbI_2, an Unforeseen Necessity in High-Efficiency Hybrid Perovskite-Based Solar Cells ?. APL Mater. 2 (2014) 091101.

[18] T. J. Jacobsson, J.-P. Correa-Baena, E. H. Anaraki, B. Philippe, S. D. Stranks, M. E. F. Bouduban, W. Tress, K. Schenk, J. Teuscher, J.-E. Moser, H. Rensmo, A. Hagfeldt, Unreacted PbI_2 as a Double-Edged Sword for Enhancing the Performance of Perovskite Solar Cells. J. Am. Chem. Soc. 138 (2016) 10331−10343.

[19] U. Kwon, M. M. Hasan, W. P. Yin, D. Kim, N. Y. Ha, S. Lee, T. K. Ahn, H. J. Park, Investigation into the Advantages of Pure Perovskite Film without PbI_2 for High Performance Solar Cell. Sci. Rep. 6 (2016) 35994.

[20] W. Li, J. Fan, J. Li, Y. Mai, L. Wang Controllable Grain Morphology of Perovskite Absorber Film by Molecular Self-Assembly toward Efficient Solar Cell Exceeding 17%. J. Am. Chem. Soc. 137 (2015) 10399−10405.

[21] S.-Y. Kim, H. J. Jo, S.-J. Sung, D.-H. Kim, Perspective: Understanding of Ripening Growth Model for Minimum Residual PbI_2 and its Limitation in the Planar Perovskite Solar Cells. APL Mater. 4 (2016) 100901.

[22] J.-H. Im, I.-H. Jang, N. Pellet, M. Grätzel, N.-G. Park, Growth of $CH_3NH_3PbI_3$ Cuboids with Controlled Size for High-Efficiency Perovskite Solar Cells. Nat. Nanotechnol. 9 (2014) 927.

[23] W. Zhu, C. Bao, F. Li, T. Yu, H. Gao, Y. Yi, J. Yang, G. Fu, X. Zhou, Z. Zou, A Halide Exchange Engineering for $CH_3NH_3PbI_{3-x}Br_x$ Perovskite Solar Cells with High Performance and Stability. Nano energy 19 (2016) 17−26.

[24] E. Zheng, X.-F. Wang, J. Song, L. Yan, W. Tian, T. Miyasaka, PbI_2-Based Dipping-Controlled Material Conversion for Compact Layer Free Perovskite Solar Cells. ACS Appl. Mater. Interfaces 7 (2015) 18156−18162.

[25] M. Yang, T. Zhang, P. Schulz, Z. Li, G. Li, D. H. Kim, N. Guo, J. J. Berry, K. Zhu, Y. Zhao, Facile Fabrication of Large-Grain $CH_3NH_3PbI_{3-x}Br_x$ Films for High-Efficiency Solar Cells via CH_3NH_3Br Selective Ostwald Ripening. Nat. Commun. 7 (2016) 12305.

[26] J. H. Noh, S. H. Im, J. H. Heo, T. N. Mandal, S. I. Seok, Chemical Management for Colorful, Efficient, and Stable Inorganic−Organic Hybrid Nanostructured Solar Cells. Nano Lett. 13 (2013) 1764−1769.

[27] D. M. Jang, K. Park, D. H. Kim, J. Park, F. Shojaei, H. S. Kang, J. P. Ahn, J. W. Lee, J. K. Song, Reversible Halide Exchange Reaction of Organometal Trihalide Perovskite Colloidal Nanocrystals for Full-Range Band Gap Tuning. Nano Lett. 15 (2015) 5191−5199.

[28] C. M. Sutter-Fella, Y. Li, M. Amani, J. W. Ager, F. M. Toma, E. Yablonovitch, I. D. Sharp, A. Javey, High Photoluminescence Quantum Yield in Band Gap Tunable Bromide Containing Mixed Halide Perovskites. Nano Lett. 16 (2016) 800−806.

[29] S. A. Kulkarni, T. Baikie, P. P. Boix, N. Yantara, N. Mathews, S. Mhaisalkara, Band-Gap Tuning of Lead Halide Perovskites Using a Sequential Deposition Process. J. Mater. Chem. A 2 (2014) 9221–9225.

[30] H.-S. Ko, J.-W. Lee, N.-G. Park, 15.76% Efficiency Perovskite Solar Cells Prepared Under High Relative Humidity: Importance of PbI_2 Morphology in Two-Step Deposition of $CH_3NH_3PbI_3$. J. Mater. Chem. A 3 (2015) 8808−8815.

[31] C. Liu, J. Fan, X. Zhang, Y. Shen, L. Yang, Y. Mai, Hysteretic Behavior upon Light Soaking in Perovskite Solar Cells Prepared via Modified Vapor-Assisted Solution Process. ACS Appl. Mater. Interfaces 7 (2015) 9066–9071.

[32] H. J. Snaith, A. Abate, J. M. Ball, G. E. Eperon, T. Leijtens, N. K. Noel, S. D. Stranks, J. T.-W. Wang, K. Wojciechowski, W. Zhang, Anomalous Hysteresis in Perovskite Solar Cells. J. Phys. Chem. Lett. 5 (2014) 1511−1515.

[33] X. Ren, Z. Yang, D. Yang, X. Zhang, D. Cui, Y. Liu, Q. Wei, H. Fan, S. F. Liu, Modulating Crystal Grain Size and Optoelectronic Properties of Perovskite Films for Solar Cells by Reaction Temperature. Nanoscale 8 (2016) 3816−3822.

Tables

Table 1. Photovoltaic performances (back scan) of prepared solar cells measured on just after preparation (left) and 3 days after preparation (right). The values are average of 8 cells.

Samples	Just after preparation				3 days later			
	J_{SC} (mA/cm^2)	V_{OC} (V)	*FF*	PCE (%)	J_{SC} (mA/cm^2)	V_{OC} (V)	*FF*	PCE (%)
2-step only	21.2	0.91	0.66	12.9	20.9	0.90	0.63	11.9
Additional MAI	22.1	0.94	0.69	14.4	22.2	0.93	0.69	14.4
Additional MA(I,Br)	20.8	0.95	0.71	14.2	20.7	0.96	0.67	13.4
Additional MABr	19.5	0.99	0.70	13.5	20.0	0.98	0.67	13.1

Table 2. Photovoltaic performances of prepared solar cells in forward scan measured on 3 days after preparation. The values are average of 8 cells.

Samples	J_{SC} (mA/cm^2)	V_{OC} (V)	*FF*	PCE (%)
2-step only	21.0	0.85	0.51	9.2
Additional MAI	22.5	0.89	0.56	11.3
Additional MA(I,Br)	21.2	0.91	0.53	10.4
Additional MABr	20.2	0.91	0.48	8.9

Figure Captions

Figure 1. Schematic illustration of the 3-step method in this study for perovskite active layer.

Figure 2. XRD patterns of prepared solar cells at the range of 2θ=10-70° and enlarged ones at 2θ=27.5–29.0°.

Figure 3. Optical properties: (a) Optical absorbance and estimated bandgaps, and (b) transmittance of prepared perovskite active layers.

Figure 4. Top-view and cross-sectional SEM images of perovskite active layers for (a,d) 2-step only, (b,e) with additional MAI and (c,f) with additional MABr spin-coating cells.

Figure 5. Typical *J-V* curves (back scan) of prepared solar cells measured on (a) just after preparation and (b) 3 days after the preparation.

Figure 6. Typical *J-V* curves of prepared solar cells in forward scan measured on 3 days after preparation.

Figure 7. Time dependence of normalized PCE for 2-step only, with additional MAI and additional MABr spin-coating cells. The solar cells were stored in air with the humidity of ~30 %.

Figures

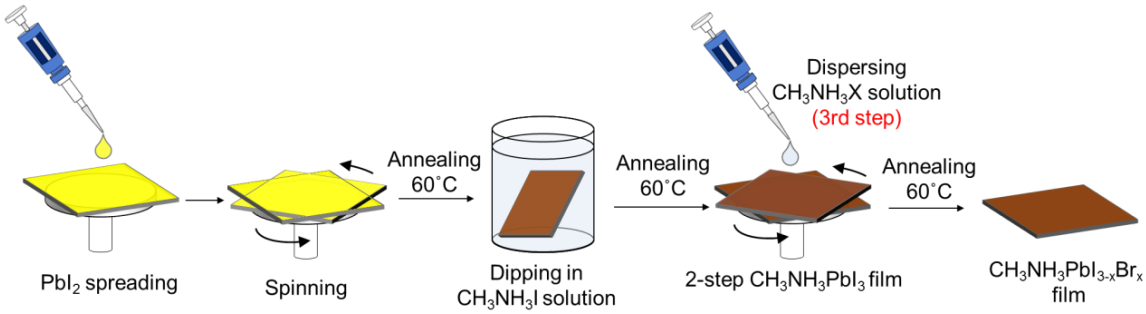

Figure 1. Schematic illustration of the 3-step method in this study for perovskite active layer.

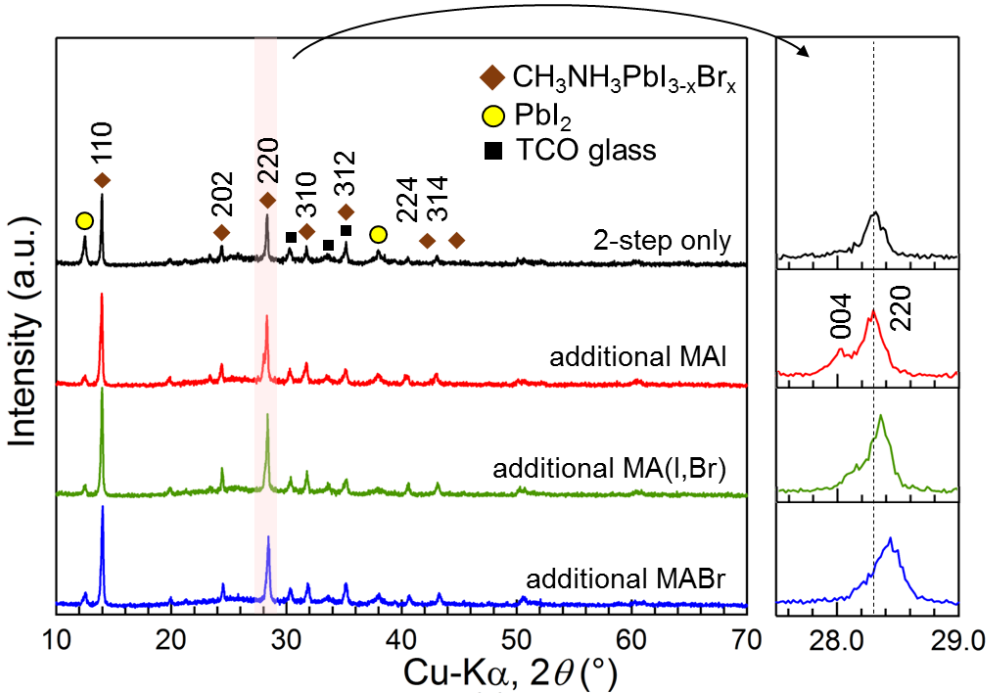

Figure 2. XRD patterns of prepared solar cells at the range of 2θ=10-70° and enlarged ones at 2θ=27.5–29.0°.

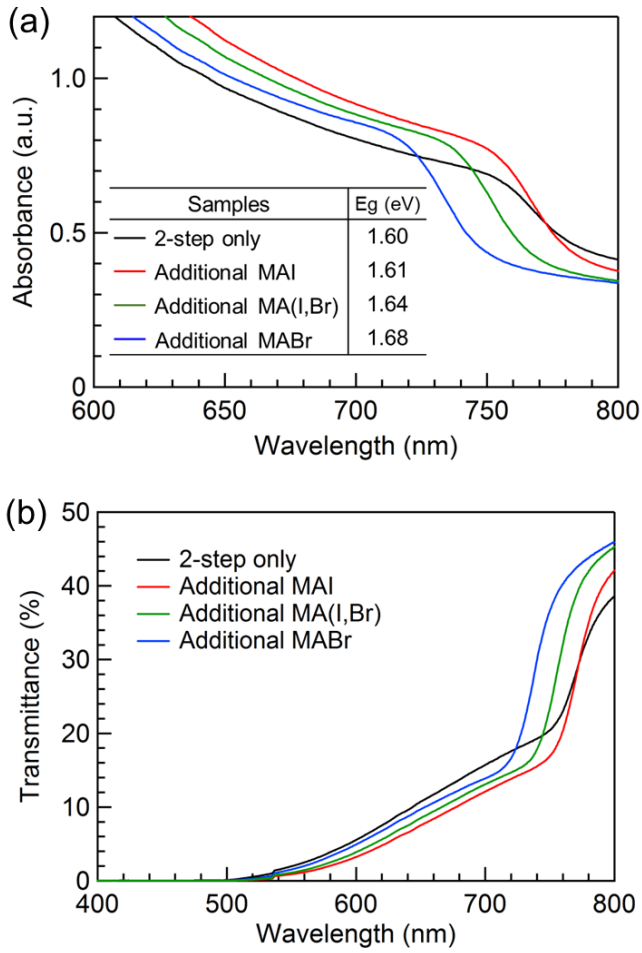

Figure 3. Optical properties: (a) Optical absorbance and estimated bandgaps, and (b) transmittance of prepared perovskite active layers.

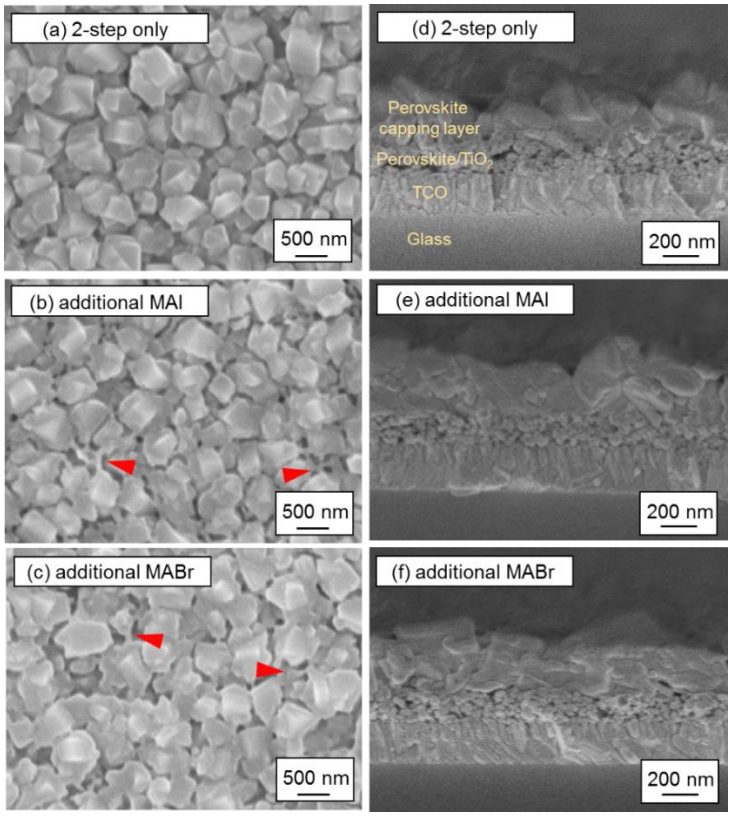

Figure 4. Top-view and cross-sectional SEM images of perovskite active layers for (a,d) 2-step only, (b,e) with additional MAI and (c,f) with additional MABr spin-coating cells.

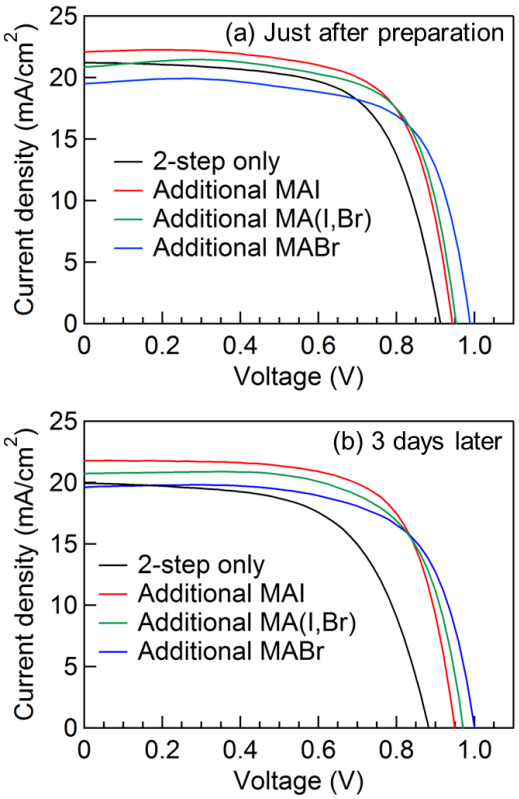

Figure 5. Typical *J-V* curves (back scan) of prepared solar cells measured on (a) just after preparation and (b) 3 days after the preparation.

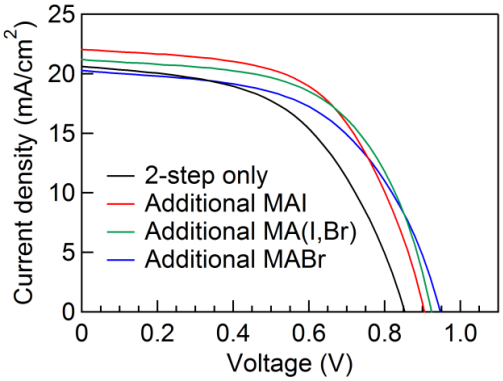

Figure 6. Typical *J-V* curves of prepared solar cells in forward scan measured on 3 days after preparation.

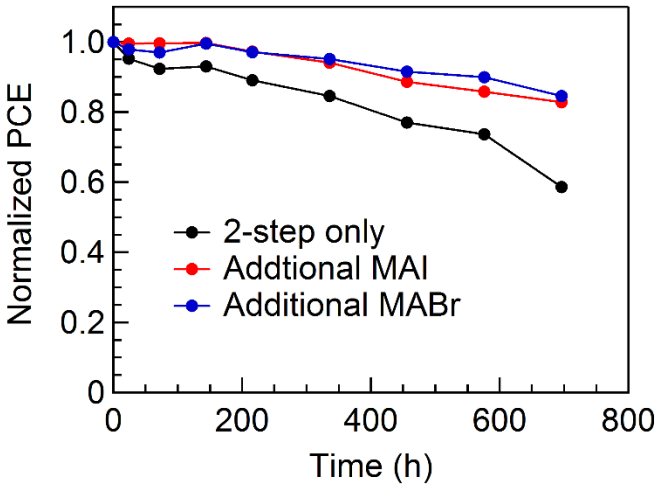

Figure 7. Time dependence of normalized PCE for 2-step only, with additional MAI and additional MABr spin-coating cells. The solar cells were stored in air with the humidity of ~30 %.

Graphical abstract

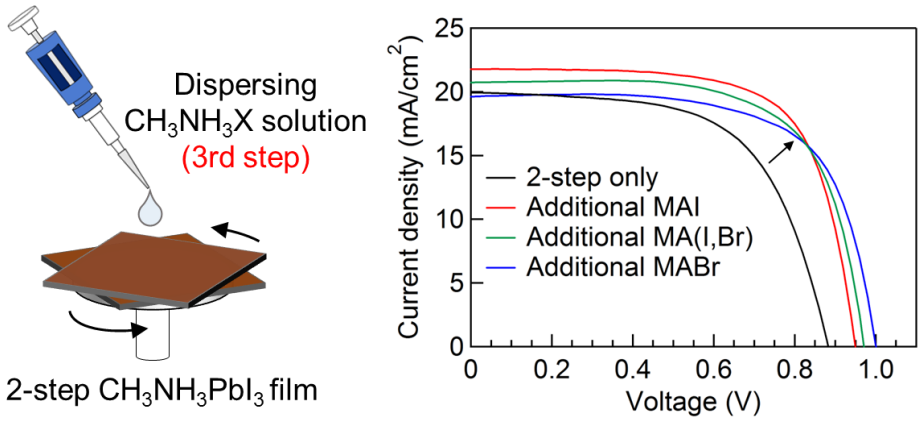

Supporting information

Perovskite Solar Cells Prepared by a New 3-step Method Including a PbI_2 Scavenging Step

Yuji Okamoto[†] and Yoshikazu Suzuki[*,‡]

[†]Graduate School of Pure and Applied Sciences, University of Tsukuba, Ibaraki 305-8573, Japan

[‡]Faculty of Pure and Applied Sciences, University of Tsukuba, Ibaraki 305-8573, Japan

Corresponding Author

* E-mail: suzuki@ims.tsukuba.ac.jp

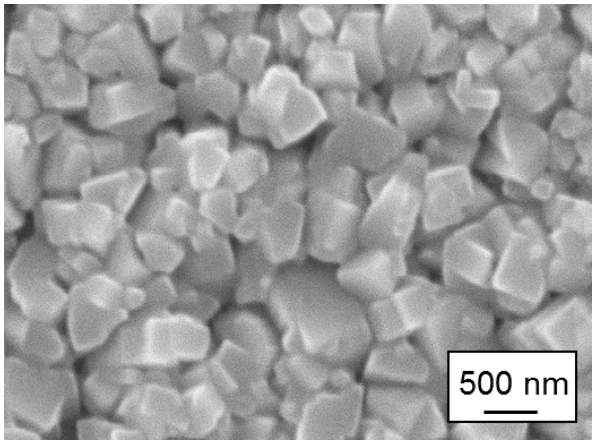

Figure S1. Top view SEM image of the perovskite active layer with additional 2-propanol spin-coating. Only 2-propanol coating, almost no change was observed.

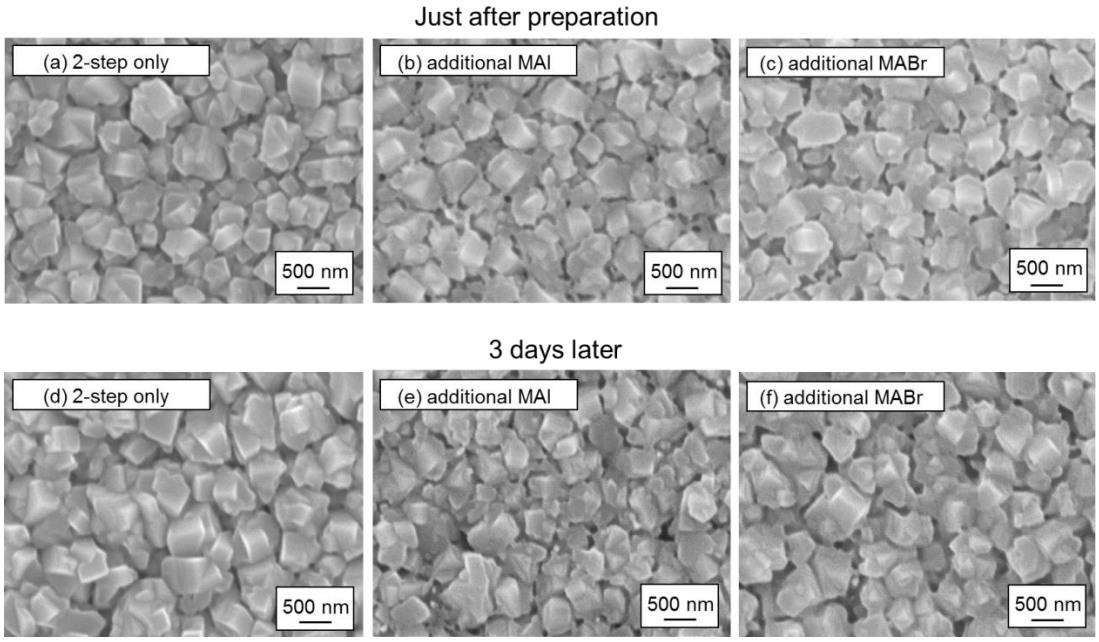

Figure S2. Top view SEM images of perovskite active layers: (a)-(c) just after preparation and (d)-(f) 3 days after preparation.